

Effects of Quenching Methods on Martensite Transformation and Shape Memory Effects of Cu-27.66Al-12.39Mn Alloy

Mahardika Sandy Ponco^{1,2}, Miftakhur Rohmah^{2,3}, Agung Imaduddin⁴, and Bondan Tiara Sofyan^{2,*}

¹Department of Mineral Chemical Engineering, Politeknik Industri Logam Morowali, Morowali 94974, Indonesia

²Department of Metallurgy and Materials, Universitas Indonesia, Kampus UI Depok 16424, Indonesia.

³Research center for Metallurgy, National Research and Innovation Agency (BRIN), Indonesia

⁴Research center for advanced materials-National Research and Innovation Agency (BRIN), Indonesia.

Abstract. Shape Memory Alloys (SMAs) exhibit unique functional properties associated with reversible martensitic transformation. This study investigates quenching methods on the microstructure and properties of Cu-27.66Al-12.39Mn (at.%) alloy. The alloy was fabricated by gravity casting, homogenized at 900 °C for 2 h with air cooling, and subsequently betatized at 900 °C for 30 min followed by three quenching routes: direct quenching (DQ), up quenching (UQ), and step quenching (SQ). The microstructure evolution of betatized sample was characterized by x-ray diffraction, optical and scanning electron microscope. The mechanical properties were evaluated by hardness and semi-empirical bending test. The alloy exhibited a $\beta 1$ (L21) microstructure in both as-cast and as-homogenized conditions, with grain growth observed. The quenching method significantly affects microstructure and hardness of Cu-Al-Mn alloy. All quenching methods resulted in partial formation of $\beta' 1$ (18R) martensite with thin plate morphology. The hardness values of DQ, UQ, and SQ samples were 366.71, 359.61, and 347.74 HVN, respectively, relating with the inverse relationship with grain size. The martensitic transformation temperature expected on cryogenic temperature (< -60 °C), so the strain recovery test at room temperature failed.

1 Introduction

Shape memory alloy (SMA) is the materials used on various industries such as aerospace industries (structural connector, vibration dampers, sealers, and pathfinder), automotive components (sensor and actuator), and biomedical (blood clot filters, heart rings and braces) [1]. SMA has a unique characteristic because of their ability to change its original shape when heated [2]. Generally, there are three types of shape memory alloy depending on their base metal, including NiTi-based, Fe-based, and Cu-Based SMA.

NiTi-based SMA introduced by Buehler et al. in 1963. This alloy called NITINOL, an abbreviation of Nickel, Titanium, and Naval Ordnance Laboratory (NOL). NiTi based SMA were applied in biomedical application such as implant orthopedy, and aerospace engineering [2]. NiTi SMA was applied in the commercial used of the clutch pipes of F-14 fighters. On biomedical, NiTi-based SMA were commonly used because of their high biocompatibility [3]. Unfortunately, NiTi-based alloy have disadvantages with their high-cost production and low transformation temperatures. Cu-based and Fe-based SMA were extensively researched as alternative alloy, regarding to shape memory effect (SME) properties.

Fe-Based SMA especially on Fe-Mn-Si alloy have potential for structural on civil engineering applications [4]. Fe-based alloy possesses high strength and ability to dumped a vibrate [5]. Fe-based SMA alloys such as Fe-

Pt, Fe-Pd, and Fe-Ni-Co showed phase transformation from γ -austenite phase (stable at high temperatures) to ϵ -martensite phase (stable at low temperatures) [6]. When cooled until room temperature after production process, this alloy has face-centered cubic (FCC) structures, if γ -austenite Fe-SMA were deformed, it will form ϵ -martensite phase.

Besides NiTi and Fe-based SMA, there are also Cu-based SMA, including Cu-Zn-Al, Cu-Al-Ni, and Cu-Al-Mn. The production cost of Cu-based SMA is lower than that of NiTi-based. Setyani et al. [1] resulted the shape memory properties of Cu-28Zn-3Al (wt.%) depended on quenching method. The up-quenching and direct-quenching methods resulted in a relatively higher shape memory effect (SME) compared to step quenching.

Cu-Al-Ni and Cu-Zn-Al possesses high shape memory effect. Unfortunately, Cu-based SMA have brittle failure because of high ordered degree and high elastic anisotropy of β -parent phase. Cu-Al-Mn with the specific composition (lower content of aluminum and high level of manganese) has good ductility caused by the lower ordered degree [7]. In addition, the Cu-Al-Mn alloys have higher transformation temperature [8].

Cu-Al-Mn alloy have austenite β -phase, which is stable at 20-30 at.% Al and temperature 560 °C. β - phase was ordered reaction and transformed to B2 and D03 / L21. The martensite was formed after quenching process. The reversible phase transformation between austenite and martensite provided shape memory effect [9]. After quenching process, 1 of 3 types of martensite

* Corresponding author: bondan@eng.ui.ac.id

namely 3R (α') 18R (β'), and 2H (γ') occurred depending on the amount of Al and Mn content. The 3R martensite formed at 20 – 22 (at.%) Al, the 18R martensite at 22 – 26 (at.%) Al, and the 2H martensite formed at 26 – 30 (at.%) Al, respectively. Mn content effected the broadened β -phase zone and improving shape memory properties [9]. The composition of CuAl-Mn have significantly affected on phase stabilization, transformation behavior, and transformation behavior [7]. The information of shape memory behavior with high aluminum and manganese content is limited. High aluminum and manganese content, especially on Cu-27.66Al-12.39Mn was investigated in this work. According to isopethal ternary phase diagram, Cu27.66Al-12.39Mn (at.%) provided single β phase and ordered transformation (β (A2) \rightarrow β 2 (B2) followed by β 2 (B2) \rightarrow β 1 (L21)) upon cooling [10]. As mentioned on previous research [1], the variation of quenching methods was significantly affected the vacancy retention, atomic order-disordered reaction, and phase transformation behavior in Cu-Al-Mn alloys [11]. The direct-quench (DQ), up-quenching (UQ) and stepquenching (SQ) were applied to obtain the martensitic transformation characteristic. Direct quenching provided the diffusional transformation process and retained a higher degree of disordered quenched alloy. The modification cooling method, such as UQ and SQ, permitted partial atomic ordering and trapped vacancy. Therefore, this study focuses on the relationship between quenching methods and the mechanical properties of the Cu-27.66Al-12.39Mn alloy.

2 Materials and methods

The Cu-27.66Al-12.39Mn (at. %) alloy was prepared by gravity casting at 1150 °C. During melting, the alloy was fluxed using borax and degassed with argon (Ar) to minimize oxidation and gas entrapment. The molten alloy was poured into an AISI H13 steel mold which is preheated at 850 °C to reduce thermal gradients during solidification. After casting, the sample was homogenized at 900 °C for 2 h to eliminate chemical segregation. This temperature was selected based on the Cu-Al-Mn ternary phase diagram, where alloys with an Al content close to 28 at.% are fully single β -phase at approximately >850 °C, avoiding the formation of secondary equilibrium phases [7]. A betatization treatment at 900 °C for 30 minutes was applied immediately prior to quenching to re-establish the disordered β (A2) phase and ensure comparable initial conditions for all samples [10]. The betatized samples were subjected into three different quenching routes, namely direct quenching (DQ), up quenching (UQ), and step quenching (SQ), in order to investigate the influence of cooling path on phase transformation and microstructure property relationships. Direct quenching (DQ) was performed by quenching the samples directly to -60 °C using an ethanol and dry-ice mixture media. Up quenching (UQ) involved an initial quench into -60 °C for 30 min, followed by reheating in boiling water at 100 °C for 30 min. Step quenching (SQ) was carried out

by quenching the samples in boiling water at 100 °C for 30 min and subsequently quenching into -60 °C using an ethanol and dry-ice mixture for 30 min. The chemical composition of investigated alloy was determined using X-ray fluorescence (XRF), and the result is summarized in Table 1.

Table 1. Chemical composition of the alloy (wt.%).

Chemical Compound	Composition (wt. %)
Al	14.2
Mn	12.917
P	0.561
Ca	0.164
Ti	<0.05
Cr	<0.05
Si	0.208
Cu	Bal.

Table 1 shows the chemical composition of the investigated alloy. After converted into (at.%), the alloy composition is Cu-27.66Al-12.39Mn.

Microstructures of the samples as-cast, as-homogenized, and as-quench were examined by optical microscope Zeiss Primotech and SEM-EDS FEI Inspect F50/Apollo X. Samples were prepared by alumina (Al₂O₃) polishing and etching using Ferro chlorine solution (5 g Fe₃Cl + 95 mL ethanol). X-Ray diffraction (XRD) using PANanalytical X'Pert Pro MPD with Cu-K α radiation was performed on as-cast, as-homogenized, and as-quench samples to identify the phases present. Vickers microhardness in compliance with ASTM E92 standard was used to examine the hardness of samples. Martensitic transformation temperature was determined by resistivity test using Oxford TeslatronPT on DQ samples. Sample was cooled until 0 K (-273 °C) using Helium (He) gas and then heated until room temperature (± 25 °C). The shape recovery test was performed on the DQ sample. Before the test, the specimen was prepared by diamond saw cutting, so the dimension was 1 \times 5 \times 40 mm. The specimen for the shape recovery test was bent in a manual jig. The measurement was done by measuring the angle formed after bending process when quenched at -60 °C (Dry ice + ethanol solution), and final angle after heating at room temperatures (± 27 °C).

3 Results and discussion

3.1 Effect homogenization process

Fig. 1 shows the microstructures of the Cu-27.66Al-12.39Mn alloy at as-cast and as-homogenized. The microstructure consists of one phase of β . The brown graded from light to dark in β phase commonly occurred in Cu-based alloys due to the influence of Cu crystallographic orientation.

Fig. 1(a) shows the microstructure of alloy on as-cast condition, indicating the structure consists of single phase with grain size of 407.17 μ m. Fig. 1(b) shows the microstructure of the alloy after homogenization process at 900 °C for 2 h. The microstructure of as-homogenized

present not significantly differences phase than as-cast, but the grain size increased to 1221.83 μm . The increased grain size of as-homogenized sample is related to the grain growth theory, where the heating process provided more energy to migrate grain boundaries, so the grain continues enlarge, reduces the number of grains, and reduces the grain boundary formed. In Cu-27.66Al12.39Mn alloy, the homogenization process decreases the hardness value. However, the high level of Al and Mn in the alloy causes the phenomenon of solid solution strengthening, so the hardness value of the alloy is higher than that of the other two alloys. The presence of grain growth causes a decrease in the hardness of the alloy after the homogenization process. Because the enlargement of the grain can reduce the limit of the grain boundary, the grain will be more easily dislocated. Beside using the optical microscope, microstructure observations were also carried out using SEM-EDS shown by Fig. 2 and Table 2.

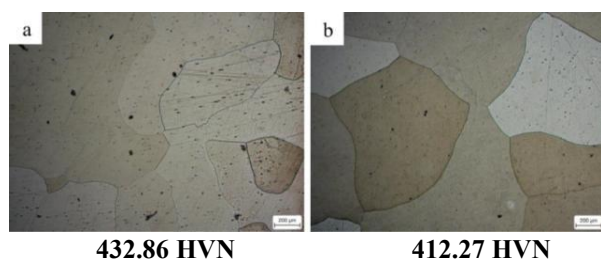


Fig. 1. Microstructures and hardness value of Cu-27.66Al-12.39Mn alloy at (a) as-cast condition, and (b) after homogenization process at 900 °C for 2 h.

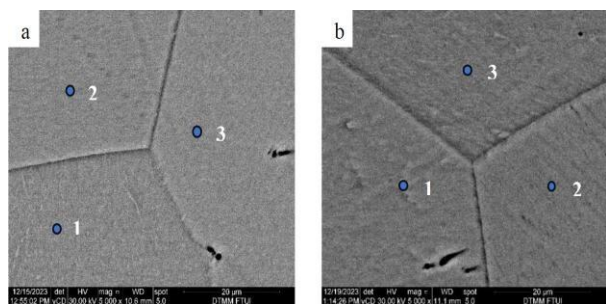


Fig. 2. SEM microstructures of Cu-27.66Al-12.39Mn alloy at condition: (a) as-cast, and (b) as-homogenized at 900 °C for 2 h.

Fig. 2 shows the alloys that both samples have single β -phase. The EDS results are listed at Table 2. In the as-cast condition, the Al content is ranged in 29.37 – 29.95 (at.%) and Mn is 13.12 – 13.80 (at.%). For the homogenized sample, Al and Mn content are not significantly different at 27.48 – 29.91 (at.%), and 13.12 – 13.80 (at.%), respectively. This is accordance with the study by Kainuma et al. [10], resulted that Mn can expand the area of phase β . Fig. 3 shows XRD diffractogram of Cu-27.66Al-13.39Mn alloy in both as-cast and as-homogenized condition. In as-cast condition, multiple peaks including reflections from the (111), (022), (133), and (024), respectively. These multiple, relatively sharp peaks indicate the presence of a polycrystalline structure with random crystallographic orientations and a high density of

internal defects and lattice distortions resulting from rapid solidification.

Table 2. EDS test result of Cu-27.66Al-12.39Mn alloy at as-cast and as-homogenized condition (900 °C for 2 hours, at spots as shown in Fig. 2).

Samples	Spots	Chemical Compound			Phase
		Cu	Al	Mn	
As-cast (Fig. 2a)	1	56.59	29.37	13.67	β_1 (L21)
	2	56.72	29.95	13.33	β_1 (L21)
	3	56.41	29.41	13.78	β_1 (L21)
As-Homogenized (Fig. 2a)	1	56.59	29.37	13.67	β_1 (L21)
	2	56.72	29.95	13.33	β_1 (L21)
	3	56.41	29.41	13.78	β_1 (L21)

In contrast, the as-homogenized sample exhibits fewer peaks but more intense and narrower peaks, particularly prominent at the (022) and (133) planes. The sharpening and intensification of specific peak, especially the (022), is consistent with grain growth and orientation alignment during prolonged thermal exposure, when crystallization reduces grain boundary energy and favors energetically preferred orientations [12]. The larger, more uniform grains in the homogenized sample support the XRD findings, confirming that grain growth and texture development occurred simultaneously. These observations are consistent with previous studies reporting that homogenization of Cu-Al-Mn alloy promotes defect annihilation and atomic redistribution within the β -phase, resulting in improved chemical homogeneity and phase stability [9]. Similar behavior was reported by Kainuma et al who demonstrated that prolonged high-temperature exposure primarily enhances β -phase ordering and structural uniformity [10].

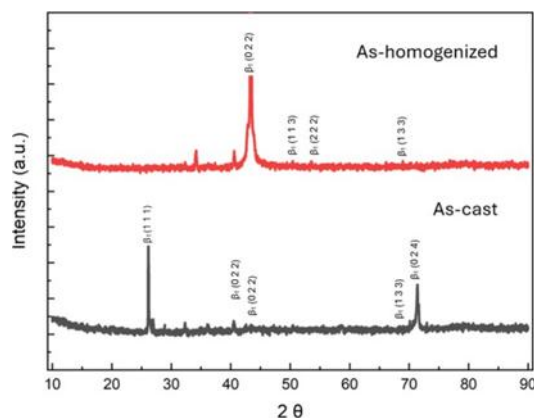


Fig. 3. X-Ray diffractogram of Cu-27.66Al-12.39Mn at as-cast and as-homogenized at 900 °C for 2 h.

3.2 Effect of quenching methods on martensite transformation

Fig. 4 shows the microstructures of Cu-27.66Al-12.39Mn after quenched with 3 different quenching methods. Fig. 4(a) shows Cu-27.66Al-12.39Mn after direct quenched, presenting a typical β_1 (L21) as matrix and martensite β'_1 (M18R). The martensite β'_1 indicated by the needle-like morphology with thin line shaped. Based on Fig. 4(b), the up-quench sample has similar microstructure with the step-quench (Fig. 4(c)),

presenting a β_1 (L21) + β'_1 (M18R) in small amount. It is seen that all microstructures are not completely martensite, indicating the martensite transformation is very cryogenic under $-60\text{ }^\circ\text{C}$. When quenched into ethanol + dry ice ($-60\text{ }^\circ\text{C}$), all sample has been passing the Ms (Martensite start) temperature but not passed the Mf (Martensite finish) temperature. So, β_1 (L21) phase is not fully transformed into martensite β'_1 (M18R).

Fig. 5 depicts the microstructure of Cu-27.66Al-12.39Mn using SEM-EDS. Based on Fig. 5, all quenched samples exhibit a single β phase. This result is consistent with the expected phase stability, referring to the alloy composition in the Cu-Al-Mn ternary phase diagram. EDS result was listed in Table 3. The direct quenched (DQ) sample has Al content in range 24.88 – 28.55 (at.%) and Mn of 13.32 – 14.47 (at.%). There are no significant changes in phase presence between as-homogenized and as-quenched conditions.

According to Fig. 6, XRD analysis of Cu-27.66Al-12.39Mn alloy subjected to DQ, UQ, and SQ reveals diffraction peak that can be indexed in β_1 (L21) and β'_1 (18R) martensitic. Differences in relative peak intensities and peak broadening are observed at the three quenching conditions. The DQ sample exhibited broader peaks with lower intensity, particularly from martensite (e.g., (220), (141)), indicate the presence of higher lattice distortion and quench-in defects induced by rapid cooling. In contrast, the UQ sample shows the sharper and more intense diffraction peaks, mainly attributed to the β_1 (L21) phase, while peak associated with the 18R martensite appears less pronounced. The SQ sample displays more evident reflections corresponding to the β'_1 (18R) phase compared to the DQ and UQ conditions, suggesting a greater tendency toward phase coexistence under intermediate cooling conditions. The observed variations in peak characteristics are attributed to differences in cooling path, which influence atomic ordering, residual lattice strain, and phase stability during quenching [12].

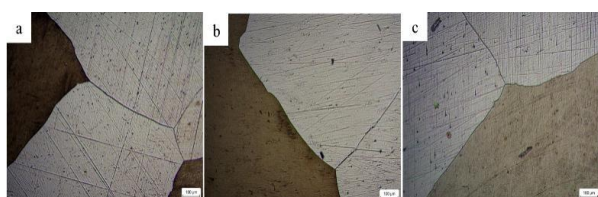


Fig. 4. Microstructure of Cu-27.66Al-12.39Mn at 100x magnification using optical microscope (a) DQ, (b) UQ, and (c) SQ condition

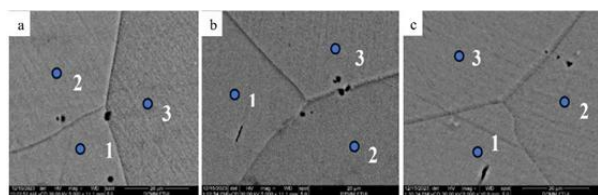


Fig. 5. SEM microstructure of Cu-27.66Al-12.39Mn in (a) DQ, (b) UQ, (c) SQ conditions.

Table 3. EDS test results of Cu-27.66Al-12.39Mn alloy after DQ, UQ, and SQ conditions obtained by SEM (at spots as shown in Fig. 5).

Samples	Spots	Chemical Compound			Phase
		Cu	Al	Mn	
DQ (Figure 5a)	1	60.65	24.88	14.47	β_1 (L21)/ β'_1 (M18R)
	2	58.59	26.94	14.47	β_1 (L21)/ β'_1 (M18R)
	3	59.64	26.18	14.18	β_1 (L21)/ β'_1 (M18R)
UQ (Fig. 5b)	1	59.30	26.69	14.01	β_1 (L21)/ β'_1 (M18R)
	2	58.55	27.53	13.92	β_1 (L21)/ β'_1 (M18R)
	3	59.10	26.40	14.40	β_1 (L21)/ β'_1 (M18R)
SQ (Fig. 5c)	1	58.25	28.20	13.55	β_1 (L21)/ β'_1 (M18R)
	2	57.14	28.55	14.32	β_1 (L21)/ β'_1 (M18R)
	3	58.88	26.89	14.23	β_1 (L21)/ β'_1 (M18R)

In Cu-Al-Mn shape memory alloys, martensitic phase stability is highly sensitive to cooling rate, and degree of atomic ordering, which might lead to the formation of metastable or transient phase configurations during non-equilibrium cooling conditions [10]. Rapid or multi-step quenching processes are known to modify the vacancy concentration and atomic disorder, potentially promoting the simultaneous appearance of diffraction features associated with different martensitic without implying a stable two-phase equilibrium state [11]. Fig. 6 presents the XRD diffraction patterns of the quenched samples. Several diffraction corresponding to the β'_1 (18R) martensitic phase were identified. In DQ sample, the (2 2 0) reflection was observed, while the UQ sample exhibited a distinct (1 4 1) peak. Meanwhile, the SQ sample showed the presence of both (2 1 2) and (1 4 1) reflections. All detected peaks are consistent with the characteristic β'_1 (18R) as referenced in the JCPDS card No. 98-015-1216.

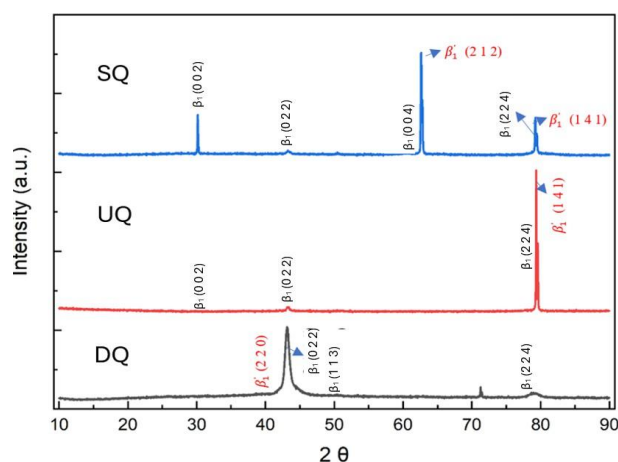


Fig. 6. XRD diffractogram of Cu-27.66Al-12.39Mn alloy in DQ, UQ, and SQ conditions.

3.3 Shape memory effect

Resistivity measurements were conducted on the Cu-27.66Al-12.39Mn alloy because the differential scanning calorimetry (DSC) test was unable to clearly detect any phase transformation at extremely low martensite start temperature (MS). Resistivity measurements are known to be more sensitive for identifying low-temperature phase transformations in Cu-based shape memory alloys. In the present study, resistivity tests were performed exclusively on DQ condition to establish a baseline reference for the temperature dependent transformation behavior under rapid cooling. The resistivity result is shown in Fig. 7, where the MS temperature is identified at approximately 210 K (-63 °C). The low MS is attributed to the relatively high Mn content of the alloy approximately ~12.39 at.%. This observation is consistent with previous studies, reporting that the martensitic transformation temperature in Cu-Al-Mn shape memory alloys is strongly dependent on Mn content. Higher Mn concentrations leading to a significant reduction in MS. Similar behavior was also reported by Kainuma et al. [8] for a Cu-17Al-12Mn (at.%) alloy, which has an MS temperature of approximately -114 °C. These results confirm that the high Mn content in the present alloy is the primary factor responsible for the very low martensitic transformation temperature. A simple bending test was conducted on Cu-27.66Al-12.39Mn after betatizing at 900 °C for 30 minutes and quenched into -60 °C dry ice + ethanol (DQ method). The result of the bending test is shown in Fig. 8.

Fig. 8 show the bending test result of the Cu-27.66Al-12.39Mn alloy after quenching. The sample fractured during the bending process, and the fracture surface exhibits a brittle character. This behavior is attributed to solid solution strengthening associated with the high Al and Mn contents in the alloy. In addition, the quenching temperature (-60 °C) is above the martensite finish (Mf) temperature, indicating that the parent β phase was not fully transformed into martensite during the test. The low Mf temperature is consistent with the influence of high Al and Mn contents, which are known to significantly reduce MS and Mf in Cu-Al-Mn alloys [8]. Consequently, the observed brittle fracture suggests limited room- temperature deformability under the present testing conditions.

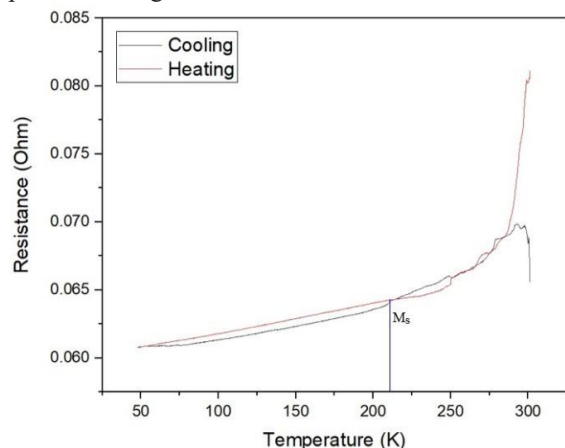


Fig. 7. Resistivity test result of Cu-27.66Al-12.39Mn alloy after quenched with DQ method.



Fig 8. Bending test result on Cu-27.66Al-12.39Mn alloy after quenched with DQ method

4 Conclusion

Based on the results of the test and observations on Cu-27.66Al-12.39Mn alloy, the conclusions are as follows:

1. Homogenization process didn't change the phase presence but enlarged the grain size from 407.17 to 1221.83 μm . The enlargement of grain size decreased the hardness values from 432.86 to 412.27 HVN.
2. The DQ, UQ, and SQ quenching methods resulted in β' (M18R) phase with thin lines morphology, but with different hardness values of 366.73, 359.61, and 347.74 HV, which are inversely proportional to the grain sizes, which are 813.37, 1048.96, 1169.96 μm , respectively.
3. The Ms temperature was -65 °C, but the Mf temperature was not able to determine, outside the detecting range of the resistivity test. The samples fractured during bending because of high brittleness.

This research was funded by Hibah BIMA – Dissertation Research Scheme in 2025 under contract number 0419/C3/DT.05.00/2025. First author wishes to extend the deepest gratitude to Tiara Annisa, for the collaborative spirit and hard work.

References

1. Setyani, I. A. Setiawan, P. R. Pamungkas, N. Sofyan, and B. T. Sofyan, "Influence of Heat Treatment on Microstructures and Shape Memory Effect of Cu-28Zn-2.5Al wt. % Produced by Gravity Casting," *International Journal of Auto. and Mech. Eng.*, **20**, no. 2, pp. 10411 – 10421, Jun. 2023, <https://doi.org/10.15282/ijame.20.2.2023.07.0805>.
2. K. Tsuchiya, "Mechanisms and properties of shape memory effect and superelasticity in alloys and other materials: a practical guide," in *Shape Memory and Superelastic Alloys*, Elsevier, 2011, pp. 3 – 14. <https://doi.org/10.1533/9780857092625.1.3>.
3. Doroftei and B. Stirbu, "Application of Ni-Ti shape memory alloy actuators in a walking micro- robot," *Mechanics*, **20**, no. 1, Mar. 2014, <http://dx.doi.org/10.5755/j01.mech.20.1.3531>.
4. Cladera, B. Weber, C. Leinenbach, C. Czaderski, M. Shahverdi, and M. Motavalli, "Iron-based shape

- memory alloys for civil engineering structures: An overview,” *Constr Build Mater*, **63**, pp. 281 – 293, Jul. 2014, <https://doi.org/10.1016/j.conbuildmat.2014.04.032>.
5. L. Janke, C. Czaderski, M. Motavalli, and J. Ruth, “Applications of shape memory alloys in civil engineering structures—Overview, limits and new ideas,” *Mater Struct*, **38**, no. 5, pp. 578 – 592, Jun. 2005, <https://doi.org/10.1007/BF02479550>.
 6. K. Hong, S. Lee, S. Han, and Y. Yeon, “Evaluation of Fe-Based Shape Memory Alloy (Fe-SMA) as Strengthening Material for Reinforced Concrete Structures,” *Appl. Sci.*, **8**, no. 5, p. 730, May 2018, <https://doi.org/10.3390/app8050730>.
 7. Y. Sutou, T. Omori, J. J. Wang, R. Kainuma, and K. Ishida, “Characteristics of Cu–Al–Mn-based shape memory alloys and their applications,” *Mater. Sci. and Eng.: A*, **378**, no. 1–2, pp. 278–282, Jul. 2004, <https://doi.org/10.1016/j.msea.2003.12.048>.
 8. W. Trehern, H. Ozcan, B. Franco, N. Hite, N. Malone, B. Loveall, T.D. Morrison, O. Benafan, I. Karaman, “Exploring thermomechanical functionality of CuAlMn as an extreme low temperature shape memory alloy,” *Mater. Letter.*, **308**, 131246, 2022, <https://doi.org/10.1016/j.matlet.2021.131246>.
 9. R. Kainuma, S. Takahashi, and K. Ishida, “Thermoelastic martensite and shape memory effect in ductile Cu-Al-Mn alloys,” *Met. and Mater. Trans A*, **27**, no. 8, pp. 2187–2195, Aug. 1996, <https://doi.org/10.1007/BF02651873>.
 10. R. Kainuma, N. Satoh, X. J. Liu, I. Ohnuma, and K. Ishida, “Phase equilibria and Heusler phase stability in the Cu-rich portion of the Cu–Al–Mn system,” *J Alloys Compd*, **266**, no. 1–2, pp. 191–200, Feb. 1998, [https://doi.org/10.1016/S0925-8388\(97\)00425-8](https://doi.org/10.1016/S0925-8388(97)00425-8).
 11. E. Obradó, L. Mañosa, A. Planes, R. Romero, and A. Somoza, “Quenching effects in Cu–Al–Mn shape memory alloy,” *Mater Sci and Eng.: A*, **273–275**, pp. 586–589, Dec. 1999, [https://doi.org/10.1016/S0921-5093\(99\)00434-7](https://doi.org/10.1016/S0921-5093(99)00434-7).
 12. S. C. Halligan, K. A. Murray, O. Vrain, J. G. Lyons, and L. M. Geever, “Controlling the Thermosensitivity of Poly(N-vinylcaprolactam) for Smart Glass Applications via Electron Beam Irradiation,” *Mater Today Proc*, **10**, pp. 430– 435, 2019, <https://doi.org/10.1016/j.matpr.2019.03.006>.